

# Nanopore-Based Protein Identification

Mazdak Afshar Bakshloo, John J. Kasianowicz,\* Manuela Pastoriza-Gallego, Jérôme Mathé, Régis Daniel, Fabien Piguet,\* and Abdelghani Oukhaled\*



Cite This: *J. Am. Chem. Soc.* 2022, 144, 2716–2725



Read Online

ACCESS |



Metrics & More

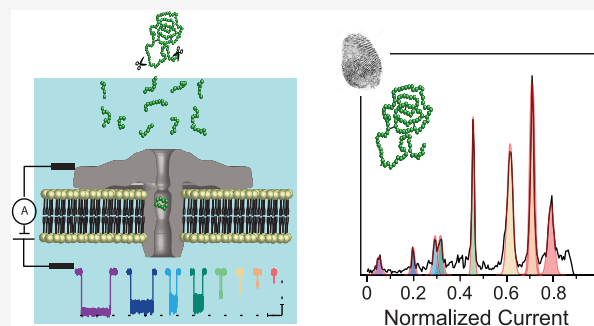


Article Recommendations



Supporting Information

**ABSTRACT:** The implementation of a reliable, rapid, inexpensive, and simple method for whole-proteome identification would greatly benefit cell biology research and clinical medicine. Proteins are currently identified by cleaving them with proteases, detecting the polypeptide fragments with mass spectrometry, and mapping the latter to sequences in genomic/proteomic databases. Here, we demonstrate that the polypeptide fragments can instead be detected and classified at the single-molecule limit using a nanometer-scale pore formed by the protein aerolysin. Specifically, three different water-soluble proteins treated with the same protease, trypsin, produce different polypeptide fragments defined by the degree by which the latter reduce the nanopore's ionic current. The fragments identified with the aerolysin nanopore are consistent with the predicted fragments that trypsin could produce.



## INTRODUCTION

Determining the identity of individual protein species in complex mixtures from biological samples is a key problem in cell biology and clinical diagnostics. If this measurement capability could be made simple, robust, automated, and low cost, it could provide research scientists with a tool to measure proteins in tissues and cells<sup>1</sup> and likely would markedly enhance medical testing at point-of-care facilities (i.e., emergency rooms and doctors' offices). Proteomics analysis techniques, such as 2-D electrophoresis,<sup>2</sup> Edman degradation,<sup>3</sup> immunoassays,<sup>4</sup> and mass spectrometry,<sup>5,6</sup> are not yet amenable for either application. In addition, unlike PCR for DNA, there is presently no high-throughput methodology for producing many copies of a single protein,<sup>7</sup> which limits the concentration at which a given protein can be detected. In this context, single-molecule proteomics approaches such as fluorosequencing,<sup>8</sup> Förster resonance energy transfer,<sup>9</sup> modified spectrometer,<sup>10</sup> tunneling current,<sup>11,12</sup> and nanopores have shown some promise.<sup>13,14</sup> Although these methods can detect single molecules, they each have a limit of detection, which needs to be determined experimentally.

Single nanometer-scale pores have been used to detect, identify, and physically characterize individual molecules (e.g., ions,<sup>15,16</sup> single-stranded oligonucleotides,<sup>17</sup> natively folded proteins,<sup>18</sup> synthetic polymers,<sup>19–21</sup> sugar molecules,<sup>22,23</sup> unfolded proteins,<sup>24–26</sup> synthetic polypeptides,<sup>27</sup> metallo-nanoparticles,<sup>28</sup> and oxidative DNA damage<sup>29</sup>) without the use of labels. The method is relatively simple; that is, the entry of a single molecule into the pore reduces the flow of ions that otherwise occurs freely through a fully open pore.<sup>17,30</sup> However, it is not merely a nanoscale version of the Coulter

counter method.<sup>31</sup> For the technique to work, two issues had to be resolved: stop the nanopores from gating<sup>15,32</sup> and have the molecules transport through the pore much more slowly than the diffusion limit.<sup>33–35</sup> The most popular application of nanopore-based single-molecule characterization is DNA sequencing, which changed the genomics landscape by offering extreme portability, very long reads, and the identification of either the nucleotides themselves<sup>17,36,37</sup> or tagged surrogates (which potentially provides far fewer base call errors).<sup>38,39</sup>

The proteomics paradigm will be positively impacted if a nanopore-based sequencing approach is applied to protein analysis. However, the latter faces many well-known challenges related to protein complexities including the heterogeneity and relatively great number of amino acid side chain residues, post-translational modifications, and the more problematic control of unfolded protein transport through the nanopore.<sup>13,40–42</sup> Unlike DNA, which has one phosphate in the polymer backbone per base, proteins are not uniformly charged, which makes the direction of polypeptide movement more random, which of course would confound any effort to sequence proteins.

To address these challenges, several nanopore approaches have been pursued including transposing the DNA strand method,<sup>40–44</sup> applying a DNA digestion sequencing techni-

Received: November 7, 2021

Published: February 4, 2022



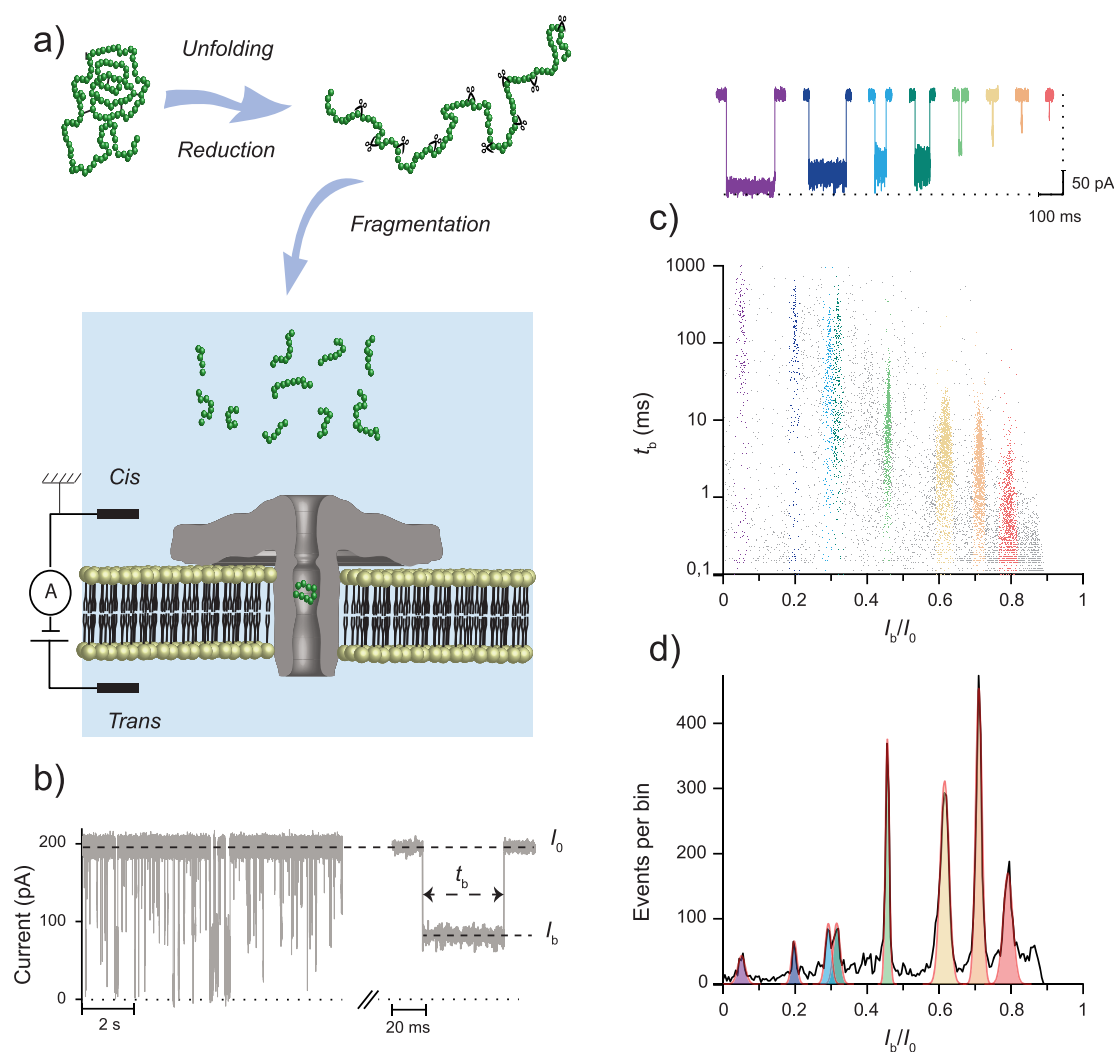


**Figure 1.** Principle of nanopore-based single-molecule spectrometry for protein fingerprinting. (a) Nanopore-based protein analysis consists first of unfolding and cleaving the protein of interest into multiple polypeptide fragment types, which are then analyzed with an aerolysin nanopore. (b) Typical ionic current time series and a single current blockade event characterized by the mean residual current  $I_b$ , the mean open current  $I_0$ , and the blockade duration  $t_b$ . (c) Scatter plot of  $t_b$  versus  $I_b/I_0$  (9685 events) where each point corresponds to a single current blockade. (d) Histogram of the  $I_b/I_0$  values. The scatter plot and the histogram both exhibit well-resolved populations caused by the interaction between the nanopore and different detectable peptide fragments generated by the enzymatic degradation of the protein to be identified. Each population of the histogram was fitted with a Gaussian distribution. A typical event is shown in the top panel for each population. The main populations are colored differently. The same color code was assigned to each main population in the scatter plot and histogram and for the typical events of each population shown in the top panel. Data were acquired in 3.6 M KCl *cis*, 4 M KCl *trans*, and 25 mM HEPES buffer, at pH 7.5, 0.2  $\mu$ M protein concentration,  $22.0 \pm 0.2$  °C, and under a +100 mV bias applied to the *trans* compartment.

que<sup>45</sup> to proteins, “sizing” of different amino acids linked to a peptide fragment,<sup>27</sup> or determining the size of single peptides.<sup>46</sup> These approaches were used to characterize polypeptide chains with single amino acid resolution,<sup>27,40,46–50</sup> detect and identify specific amino acids,<sup>45,51,52</sup> and detect subtle chemical modifications<sup>27,40,53–55</sup> or post-translational modifications,<sup>56–58</sup> but have not been able to read an entire protein’s sequence.

As protein sequencing remains an unmet challenge, protein identification by single-molecule fingerprinting methods are being considered.<sup>13</sup> These techniques involve comparing a measured protein signal to a database of known protein signatures. Although this requires the use of large databases and provides a less detailed picture of protein composition than the sequencing approach, it is of great interest,

particularly because of its relative technical simplicity compared to sequencing.

Several computational studies showed the feasibility for whole-proteome identification with high confidence through single-molecule fingerprinting (based on either nanopore measurements,<sup>59,60</sup> fluorosequencing,<sup>61</sup> or Förster resonance energy transfer<sup>62</sup>) coupled with deep learning artificial intelligence strategies. For instance, it has been predicted, when using solid-state nanopores coupled to labeled analytes, that more than 95% of the proteins in the human proteome can be identified by labeling the same set of three amino acid residues.<sup>59</sup> More recently, it was demonstrated computationally that 97.9% of the proteins in the human proteome can be identified using biological nanopores when detecting fragments from enzymatic degradation of unlabeled proteins.<sup>60</sup> One study with a solid-state nanopore suggests that physical theory

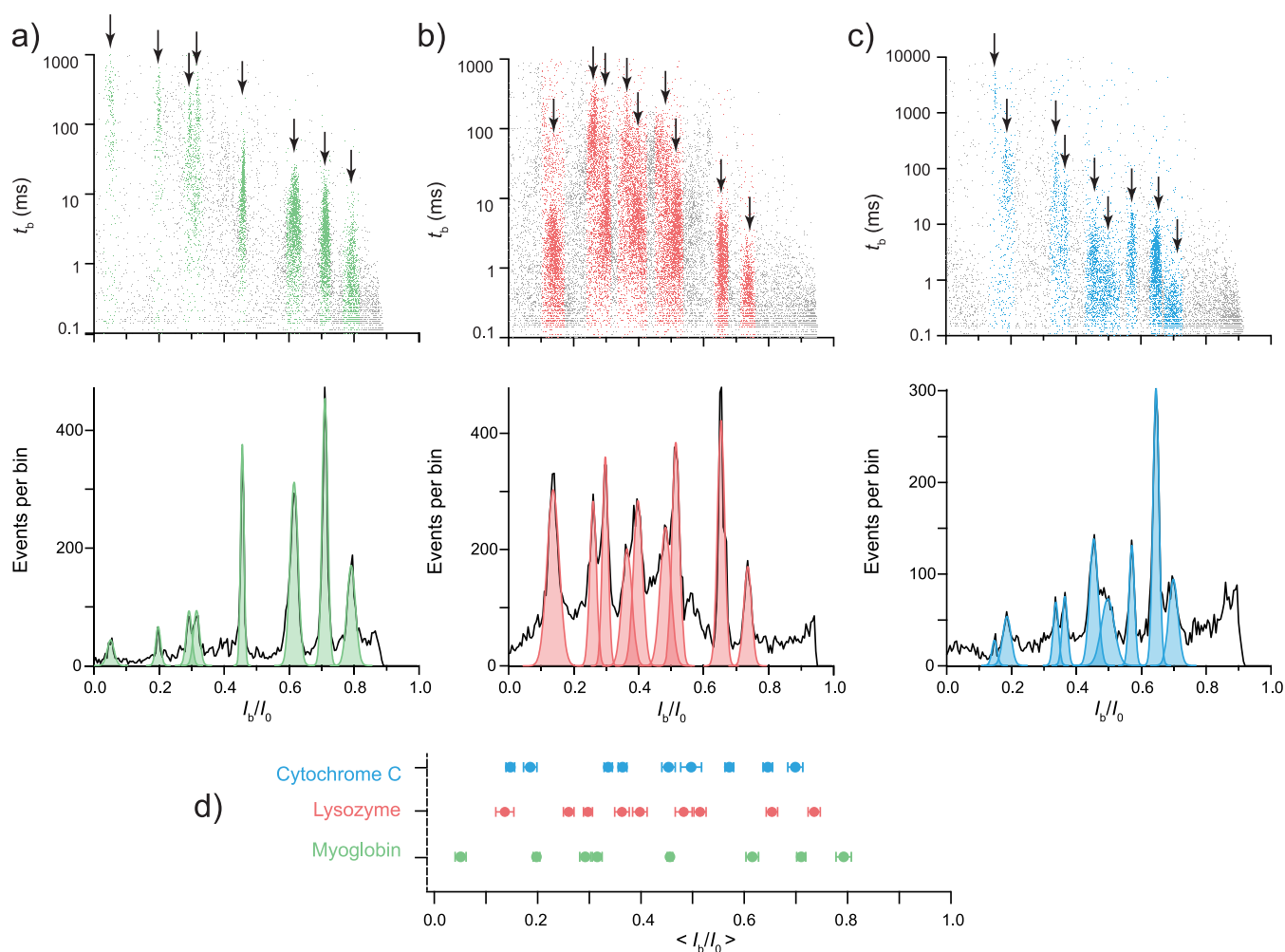


**Figure 2.** Fragmentation profiles of different proteins. (Top) Scatter plot of  $t_b$  versus  $I_b/I_0$  and (bottom) histogram of  $I_b/I_0$  values in the case of three different proteins, (a) myoglobin ( $N = 9685$ ), (b) lysozyme ( $N = 23818$ ), and (c) cytochrome  $c$  ( $N = 9103$ ), obtained with the aerolysin nanopore ( $N$  indicates the number of detected events for each protein). Each population of histograms was fitted with Gaussian mixtures. The scatter plot and histogram of each protein exhibit well-resolved populations corresponding to different peptide fragments (the main populations are indicated with arrows). (d) Comparison of the  $\langle I_b/I_0 \rangle$  values of the main populations for the three different proteins. The error bars correspond to the standard deviation of a Gaussian fit of the corresponding population in the  $I_b/I_0$  histogram. All data were acquired in 3.6 M KCl *cis*, 4 M KCl *trans*, and 25 mM HEPES buffer, at pH 7.5, 1  $\mu$ M (lysozyme or cytochrome  $c$ ) or 0.2  $\mu$ M myoglobin protein concentration,  $T = 22.0 \pm 0.2$  °C, and  $V = +100$  mV applied to the *trans* compartment.

(rotational dynamics) might prove useful to identify proteins, at the single-molecule level, when they are bound to a site inside the pore.<sup>63</sup>

Here, we demonstrate a technique for protein fingerprinting at the single-molecule level, by combining nanopore technology with an approach analogous to the existing standard mass-spectrometry-based protein identification method, where copies of the protein to be identified are cleaved into peptide fragments, the products are subsequently analyzed, and the results are compared to a signal database of known proteins to identify the target protein. Some of our initial findings were reported elsewhere,<sup>64</sup> and Maglia's group showed a similar proof-of-concept using the Frac nanopore<sup>65</sup> at the time of the present work's submission.

## RESULTS AND DISCUSSION

### Nanopore-Based Protein Fingerprinting Approach.

Our goal is to identify proteins by detecting their enzymatically cleaved fragments using a nanopore. We deemed this feasible because it was shown that a single biological nanopore can

detect the enzymatic digestion of biopolymers in the bulk. Specifically, the *Staphylococcus aureus*  $\alpha$ -hemolysin channel was used to detect, in real time, the RNase A-induced cleavage of poly(U) oligonucleotides into ever smaller random length polymers, and the negative control with poly(A) homopolymers, which are not substrates for RNase A, worked as predicted (i.e., no poly(A) cleavage products were detected).<sup>17</sup>

To test the possibility that nanopores could also detect enzyme-produced protein fragments, we first used the  $\alpha$ -hemolysin nanopore, trypsin, and a short polypeptide sequence (e.g., the first 40 N-terminus amino acid residues of the *Bacillus anthracis* lethal factor protein<sup>66</sup>). At pH 5.5, trypsin should have produced five positive, three neutral, and three negative polypeptide fragments. The results demonstrated that the uncleaved polypeptide produced essentially no nanopore current blockades (data not shown). After adding trypsin, we observed three peaks in the mean normalized residual current histogram (Supplementary Figure 1), when the applied potential would electrophoretically drive net negatively charged molecules into the pore. Because the mean residence

times of synthetic polymers and short single-stranded DNA oligomers are much greater in the AeL pore than in the channel formed by  $\alpha$ -hemolysin,<sup>19,21,33</sup> we used AeL to analyze the three target native proteins in this study.

Figure 1a demonstrates that when a native protein of interest is first unfolded and then digested with trypsin, the resultant polypeptide fragments can readily be detected with an AeL nanopore. A typical ionic current recording segment, which illustrates the interaction of different peptide fragments with +100 mV applied voltage, is shown in Figure 1b. The measured quantities (the mean residual current  $I_b$  or its value relative to the mean open pore current  $I_b/I_0$  and the fragment-induced blockade duration  $t_b$ ) are shown for a typical event. The corresponding scatter plot of  $t_b$  as a function of  $I_b/I_0$  and the histogram of the  $I_b/I_0$  values are shown in Figure 1c and d, respectively. Both the scatter plot and histogram show eight well-separated peaks, which correspond to distinct fragment populations with easily discernible  $I_b/I_0$  values. These populations correspond to the interaction of physically distinct, different peptide fragments from the enzymatic digestion of the target protein, with the AeL nanopore. Typical well-resolved events for each population are shown in the top panel. We show below that the identity of the target protein is defined by the number of polypeptide fragment populations and their mean  $I_b/I_0$  values ( $\langle I_b/I_0 \rangle$ ).

To critically evaluate the potential use of AeL nanopores for discriminating between different proteins, we analyzed three target proteins with roughly similar molecular masses, myoglobin (16.9 kg mol<sup>-1</sup>), lysozyme (14 kg mol<sup>-1</sup>), and cytochrome *c* (12 kg mol<sup>-1</sup>), which were each denatured and then subjected individually to proteolysis by the same enzyme, trypsin. The corresponding  $t_b$  versus  $I_b/I_0$  scatter plot and  $I_b/I_0$  histogram for each protein exhibit well-defined populations of specific  $\langle I_b/I_0 \rangle$  values, which correspond to different types of detectable polypeptide fragments (Figure 2a–c, respectively). The number of polypeptide fragment populations and their respective  $\langle I_b/I_0 \rangle$  values are shown in Figure 2d for each of these native target proteins. The results clearly show that these measurements constitute a sufficient criterion to discriminate between the native proteins. The reproducibility of the approach was assessed with three independent nanopores for each native protein. The corresponding  $I_b/I_0$  histograms are shown for myoglobin (Figure 3) and cytochrome *c* and lysozyme (Supplementary Figures 2 and 3, respectively). The number of peptide fragment populations and their  $\langle I_b/I_0 \rangle$  values were highly reproducible for each target protein.

While the number and positions of the  $\langle I_b/I_0 \rangle$  populations are clear criteria for nanopore-based fingerprinting of proteins, it is possible that, considering the estimated number ( $>2 \times 10^4$ ) of different proteins in the human proteome,<sup>67</sup> several protein profiles based only on this measurement might overlap. To address this issue, additional current blockade event statistical properties, as well as different experimental conditions (see the Conclusion section), could be explored to decipher ambiguous profiles. Among the blockade properties, one may consider for each  $I_b/I_0$  population  $j$  the distribution of blockade durations ( $t_b$ ) <sub>$j$</sub>  and the distribution of residual current standard deviations ( $\sigma_b$ ) <sub>$j$</sub>  (Figure 4 and Supplementary Figures 4, 5, and 6), which provide additional characteristic and reproducible information to refine the signature of each initial protein. As an illustration, Supple-

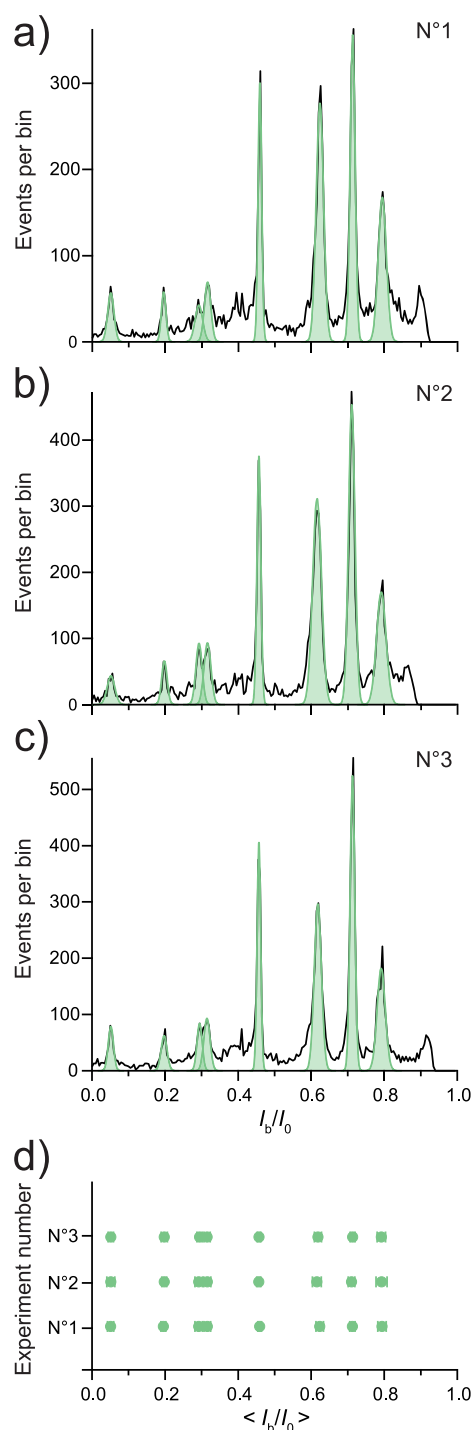


**Figure 3.** Reproducibility of the fragmentation profile of myoglobin through the aerolysin nanopore. Histograms of  $I_b/I_0$  values (8452, 9685, and 10 023 events from (a) to (c)) in the case of independent experiments with three single nanopores performed under the same experimental conditions (3.6 M KCl *cis*, 4 M KCl *trans*, and 25 mM HEPES buffer, at pH 7.5, 0.2  $\mu$ M myoglobin protein concentration,  $T = 22.0 \pm 0.2$  °C, and  $V = +100$  mV applied to the *trans* compartment). (d) Comparison of the  $\langle I_b/I_0 \rangle$  values of the main populations for the experiments performed with three different AeL nanopores. The error bars correspond to the standard deviation of a Gaussian fit of the corresponding population in the  $I_b/I_0$  histogram.

mentary Table 2 shows the protein fingerprinting ID of the three proteins analyzed here.

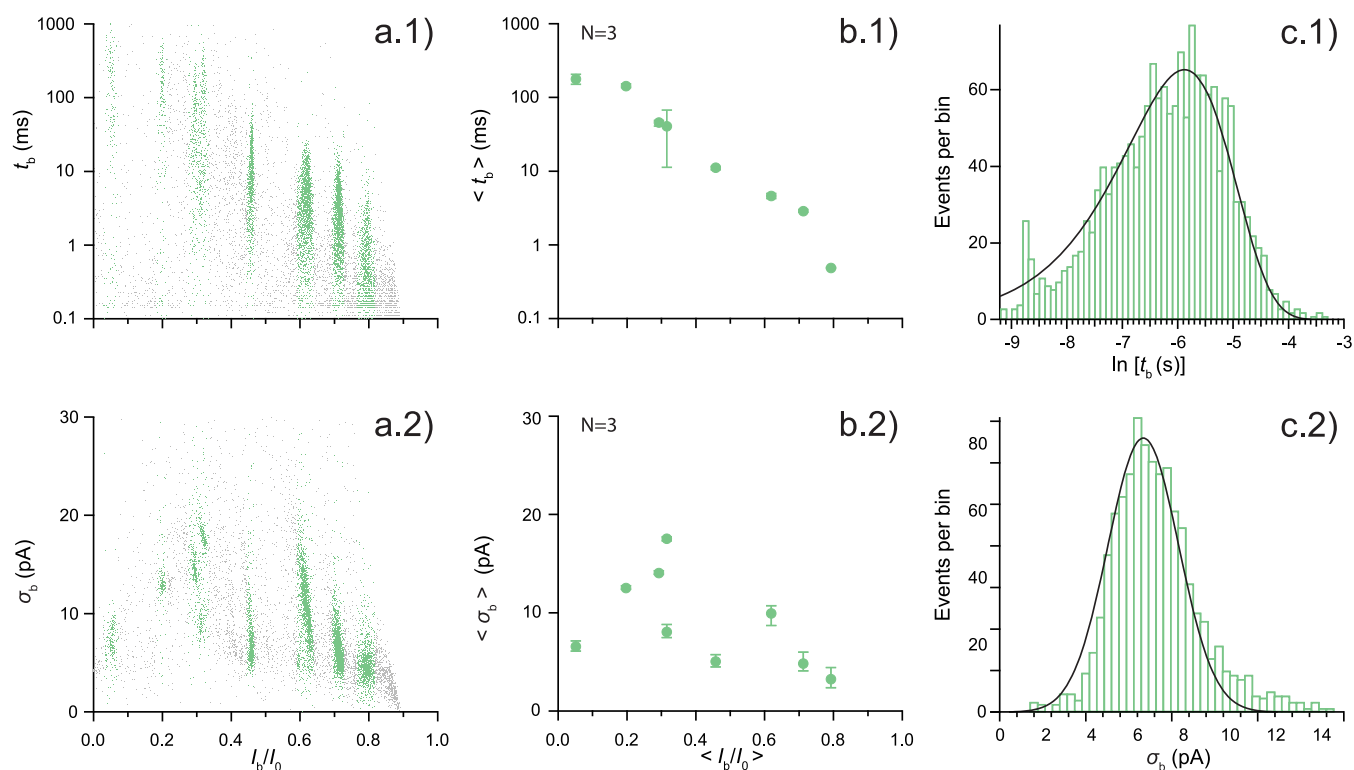


**Figure 4.** Additional blockade properties refine the protein's fingerprint. Analysis of the fragmentation profile of myoglobin. (a.1, b.1, c.1) Analysis of blockade duration  $t_b$ : (a.1) Scatter plot of  $t_b$  versus  $I_b/I_O$  ( $N = 9685$ ). (b.1)  $\langle t_b \rangle$  versus  $I_b/I_O$  of each population of single experiments reaveraged over three independent experiments. Error bars extend to the lowest and the highest  $\langle t_b \rangle$  values measured in independent experiments for each population. (c.1) Typical distribution of  $\ln(t_b)$  values for a given  $I_b/I_O$  population. The solid black line is a distribution fit corresponding to a single-exponential probability density model, where the maximum occurs at  $\ln(\langle t_b \rangle)$ . (a.2, b.2, c.2) Analysis of standard deviation  $\sigma_b$  of residual current: (a.2) Scatter plot of  $\sigma_b$  versus  $I_b/I_O$  ( $N = 9685$ ). (b.2)  $\langle \sigma_b \rangle$  versus  $I_b/I_O$  value of each population of single experiments reaveraged over three independent experiments. The error bars extend to the lowest and the highest  $\langle \sigma_b \rangle$  values measured in independent experiments for each population. (c.2) Typical distribution of  $\sigma_b$  values for a given  $I_b/I_O$  population; the solid black line is a Gaussian fit to the data.

**Polypeptide Capture Mechanism.** This capability clearly requires that a sufficient number of different types of polypeptide fragments enter the pore. To gain insight into the underlying physical mechanisms for polypeptide capture by the AeL nanopore, we compared the blockade frequency of myoglobin fragments with both polarities of the applied potential (Figure 5). For  $\Delta V < 0$ , only a few peptide-induced current blockades per unit time are detected, in marked contrast to the results obtained with  $\Delta V > 0$ . Qualitatively similar results were obtained with the other proteins (see Supplementary Figure 7). This strong asymmetry indicates a predominant role of voltage-dependent forces in polypeptide entry (for details see note 1 in the Supporting Information).

For a given initial protein, we compared the measured blockade populations to the theoretical trypsin-induced peptide fragments (Figure 6). Indeed, theoretically, cleavage by trypsin should have produced 23, 24, and 23 polypeptide fragments for myoglobin, lysozyme, and cytochrome *c*, respectively. However, the AeL nanopore detected fewer (i.e., 8, 9, and 9) different fragments (Figure 6), based on the degree by which the polymers reduce the pore conductance with related blockade duration distributions. Two major forces that could overcome the geometric entropy barrier to polymer capture by a nanopore<sup>68,69</sup> are electrophoresis (e.g., for oligonucleotide capture by the  $\alpha$ -hemolysin nanopore<sup>17,70</sup>) and electroosmotic flow (EOF) (e.g., for capture of electrically neutral cyclodextrins in the  $\alpha$ -hemolysin and AeL pores<sup>71</sup>). A detailed analysis of the peptide fragment capture data reported

here is presented in the Supporting Information, but based on the applied voltage polarity, polypeptide net charge, and size detection threshold, the results suggest that EOF plays a significant role in peptide capture and transport in the AeL pore. EOF can allow polypeptide fragments with different net electrical charges toward the nanopore (even possibly against electrophoresis), thus increasing the potential number of fragments contributing to the signature of the initial protein. The details of polypeptide capture physics notwithstanding, it is clear that similar molecular mass proteins can be discriminated by the AeL nanopore even without detecting all of the fragment types.

## CONCLUSION

We demonstrated the ability of the AeL nanopore to discriminate between different native proteins based on the signals generated by trypsin-induced polypeptide fragments. While the three proteins studied here are similar in molecular mass, the method should work well without limitation of the size, conformation, and charge of the protein. Moreover, the present method is easier to implement, rapid, inexpensive, user-friendly, and label-free. It also avoids cumbersome sample preparations compared to conventional methods and most other single-molecule techniques. In addition, it can be quantitative, because the capture rates of the different polypeptides should be proportional to their concentrations. As is true with other fingerprinting methods, this method requires access to large databases. Nevertheless, our technique

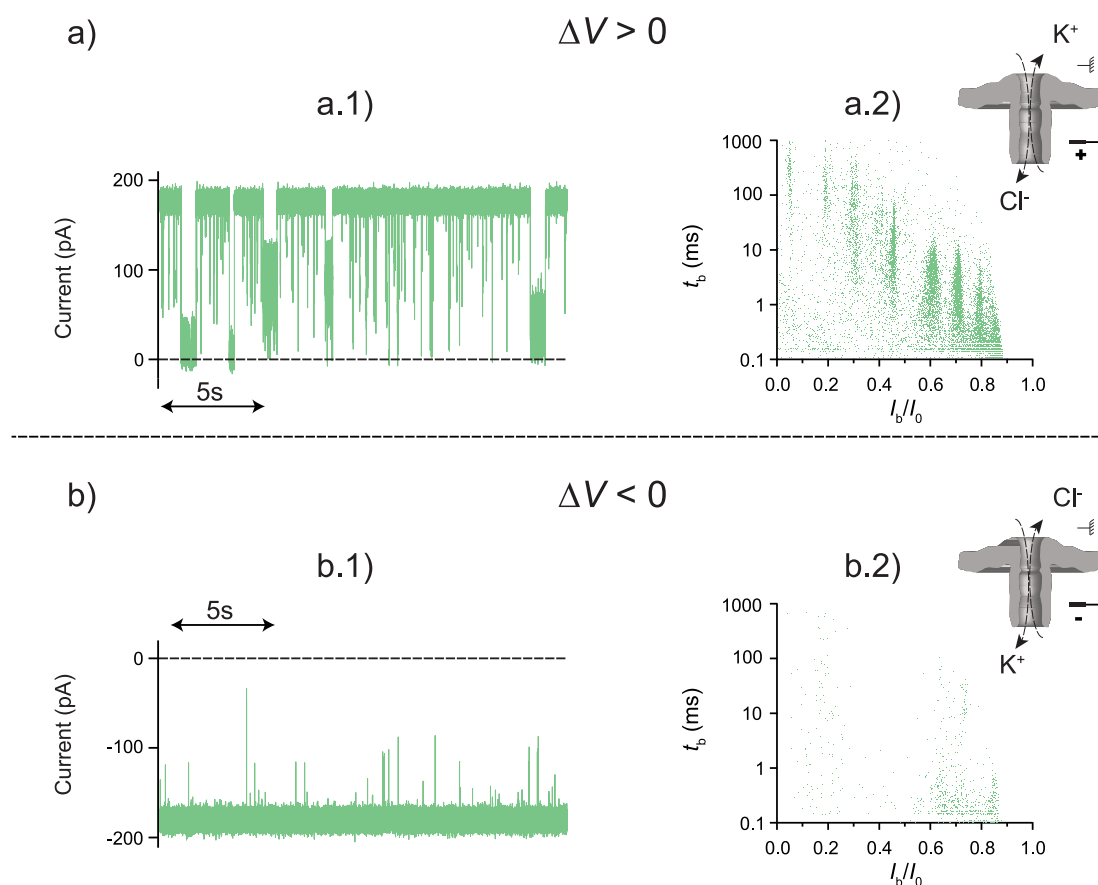


**Figure 5.** Effect of voltage polarity on myoglobin polypeptide fragment capture. (a) Positive polarity. A positive *trans* voltage induces a flow of anions from the *cis* to the *trans* compartment and a flow of cations in the opposite direction. (a.1) Representative segment of a typical current versus time recording and (a.2) corresponding  $t_b$  versus  $I_b/I_0$  scatter plot. (b) Negative polarity. (b.1) Portion of a typical current versus time recording and (b.2) corresponding  $t_b$  versus  $I_b/I_0$  scatter plot. Data were acquired in 3.6 M KCl *cis*, 4 M KCl *trans*, and 25 mM HEPES buffer, at pH 7.5, 0.2  $\mu$ M myoglobin concentration,  $T = 22.0 \pm 0.2$  °C, and  $V = +90$  mV (a) and  $-90$  mV (b).

could be immediately and easily be integrated into existing high-throughput nanopore platforms and could find immediate application for protein identification in the context of clinical applications and life sciences.

In addition to using the above criteria (specific  $\langle I_b/I_0 \rangle$  values, plus the residence time and blockade event standard deviation distributions) to discriminate between different proteins based on fragment-induced nanopore current blockade patterns, varying the experimental conditions, including applied potentials (to change part of the driving force for capturing the polypeptide fragments), electrolyte concentration (to alter electrostatic interactions of the polypeptides with the nanopore), different pH values (to change the net charge on the polypeptide fragments), temperature (to alter the nanostructures within the fragments), and/or different proteases (to cleave the proteins into different fragments), will likely provide additional discrimination capability. We are currently exploring those possibilities. Nevertheless, the ability of the AeL nanopore to discriminate between three different proteins with approximately the same molecular mass is clear.

## EXPERIMENTAL SECTION

**Aerolysin Production.** AeL is a pore-forming toxin from *Aeromonas hydrophila* produced as the precursor protein proaerolysin (ProAeL), which forms soluble dimers.<sup>72,73</sup> Recombinant wild-type ProAeL was produced in *Escherichia coli* BL21 using the pET22b-PA vector. ProAeL is produced after IPTG induction and localizes into

the bacteria periplasm. The periplasmic fraction containing soluble ProAeL dimers was extracted using an osmotic shock.<sup>74</sup> Because the recombinant protein is C-terminal His-tagged, ProAeL was further purified by affinity chromatography using Ni-Sepharose MiniSpin columns and elution was made by adding imidazole. The recombinant ProAeL purity (about 99%) was determined by SDS-polyacrylamide gel electrophoresis and Coomassie blue staining. The ProAeL concentration was estimated by optical absorbance at 280 nm. ProAeL was activated by trypsin digestion (5:3 ProAeL:trypsin mass ratio) and stored at 4 °C for up to one month.

**Proteins, Enzymes, and Aqueous Buffers.** His SpinTrap mini columns were purchased from GE Healthcare Life Science (Chicago, IL, USA), and IPTG (R0392) and HEPES buffer (BP310) from Thermo Fisher Scientific (Waltham, MA, USA). Cytochrome *c* (C2506), lysozyme (L6876), myoglobin (M0630), guanidine hydrochloride (G4505), trypsin solution (T1426), imidazole (I04716), potassium chloride (P5405), and decane (457116) were purchased from Merck (Darmstadt, Germany). Dithiothreitol (DTT, 10708984001), diphytanoyl-phosphocholine (DPhPC, 850356P), and tris(hydroxymethyl) aminomethane (TRIS, 28808.294) were purchased from Roche (Basel, Switzerland), Avanti Polar Lipids (Alabaster, AL, USA), and VWR (Radnor, PA, USA), respectively.

**Protein Digestion.** Cytochrome *c*, lysozyme, and myoglobin (280  $\mu$ M) were denatured with 3.6 M GdnHCl and reduced with 5 mM DTT for 45 min at 25 °C under 300 rpm stirring. The solution was subsequently diluted 5-fold with 100 mM Tris-HCl buffer at pH 7.5. Each protein was digested by trypsin in a 1:20 ratio (protein:trypsin, mass:mass) for 16 h at 37 °C under 300 rpm stirring. Trypsin cleavage was stopped by quenching the sample in ice. The fragmented proteins were analyzed with the nanopores the same day.

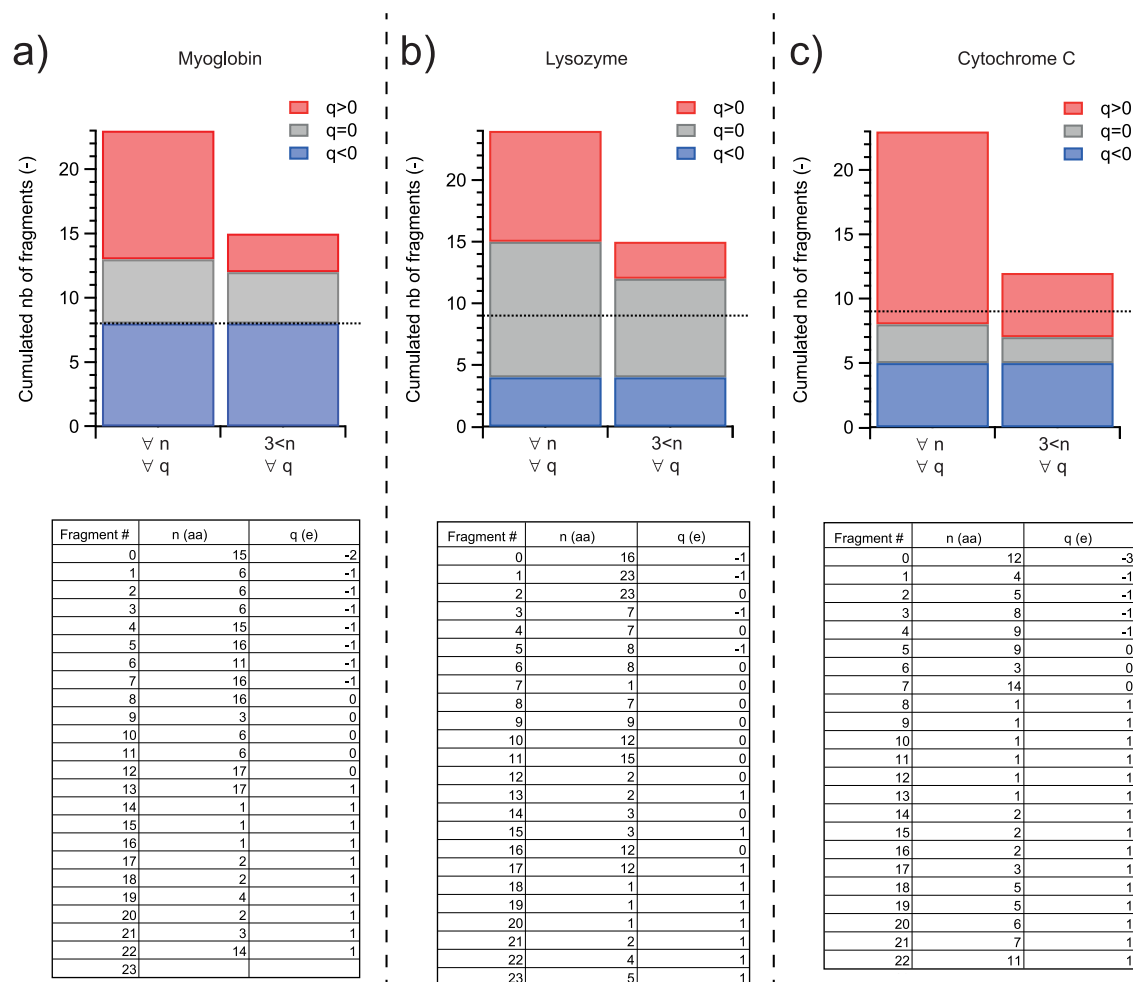


**Figure 6.** Theoretical versus detectable fragments. (Top) Category plot of the cumulative number of theoretical fragments generated by trypsin-specific degradation of the initial protein myoglobin (a), lysozyme (b), and cytochrome *c* (c). The color code is assigned to the net charge  $q$  of the fragment: blue for negatively charged, gray for neutral, and red for positively charged fragments. For each plot, the first category gathers all peptide fragments independently of their number of amino acids  $n$  and charge; the second one gathers all peptide fragments strictly longer than three amino acids (aa) independently of their charge. For each graph, the horizontal line indicates the number of populations measured. (Bottom) For each protein, the table details the values of  $n$  and  $q$  of each fragment.

**In Silico Modeling of Protein Digestion.** In silico modeling of each protein's fragmentation by trypsin was calculated using the free software exPASy PeptideCutter ([https://web.expasy.org/cgi-bin/peptide\\_cutter/peptidecutter.pl?I7CLV3](https://web.expasy.org/cgi-bin/peptide_cutter/peptidecutter.pl?I7CLV3)). The codes of the analyzed proteins (myoglobin: P68082, lysozyme: P00698, cytochrome *c*: P00004) are available in a free Uniprot database (<https://www.uniprot.org>). For each protein, the number, sequence, number of amino acids, mass, and electrical charge of the peptide fragments are listed (Supplementary Table 1).

**Nanopore Recording.** A vertical lipid bilayer setup (Warner Instruments, Hamden, CT, USA) was used for all the experiments with AeL. The lipid bilayer was formed by painting and spontaneous thinning a film of DPhPC in decane (10 mg/mL) over a 150  $\mu\text{m}$  diameter aperture separating the *cis* and *trans* compartments. The aqueous solutions on both sides of the membrane contained 1 mL of 4 M KCl and 25 mM HEPES at pH 7.5. Two Ag/AgCl electrodes were used to apply +100 mV across the membrane and measure the ionic current. The *cis* compartment is defined as the virtual ground. After forming the lipid bilayer, activated aerolysin was added to the *cis* compartment at  $\sim 50$  ng/mL final concentration. Once a single AeL nanopore formed, 100  $\mu\text{L}$  of a fragmented protein sample (i.e., either myoglobin, lysozyme, or cytochrome *c* that had been treated with trypsin) was added to the *cis* compartment at a final protein concentration of 0.2  $\mu\text{M}$  for myoglobin and 1  $\mu\text{M}$  for lysozyme or cytochrome *c* (thus diluting the *cis* compartment to 3.6 M KCl).

Single-channel current recordings were performed using an Axopatch 200B patch-clamp amplifier (Molecular Devices, Sunnyvale, CA, USA) in the whole-cell mode with a CV-203BU headstage. The signal was filtered using the internal 4-pole Bessel filter at a cutoff frequency of 10 kHz. The data were digitized at 100 kHz and current digital resolution of 30.5 fA/bit state, using a DigiData 1550B A/D-converter (Molecular Devices) controlled by Clampex 10.2 software (Molecular Devices). The solution temperature was held at  $22.0 \pm 0.2$   $^{\circ}\text{C}$  for all the experiments with a Peltier device controlled by a bipolar temperature controller (CL-100, Warner Instruments) coupled to a liquid cooling system (LCS-1, Warner Instruments).

Single  $\alpha$ -hemolysin channels were formed by adding that pore-forming toxin to the *cis* side of DPhPC membranes on an Electronic BioSciences quartz nanocapillary (San Diego, CA, USA). The aqueous electrolyte solution contained 4 M KCl, and the ionic current was measured with an Electronic BioSciences patch clamp amplifier. The N-terminal fragment of *B. anthracis* lethal factor (with the following amino acid residues: AGGHGDVGMH VKE-KEKNKDE NKRKDEERNK TQEEHLKEIM) was added to the *cis* solution. Because the original polypeptide was short, a denaturant was not added. Trypsin was subsequently added to the *cis* side, and the transient current blockades caused by protease-induced polypeptide fragments were detected by threshold discrimination with in-house software (e.g., ref 17), despite the fact that trypsin activity is reduced at high ionic strength.<sup>75</sup> The current blockade histogram plot

(Supplementary Figure 1) was created by computing the mean current for each event and calculating the ratio of those mean current values to the mean fully open nanopore current.

**Data Analysis.** Data analysis for the AeL nanopore was performed using Igor Pro 6.12A software (WaveMetrics, OR, USA) with in-house routines. The approach relies on a statistical analysis of the properties of the analyte-induced current blockades, involving at least several hundreds (more typically thousands) of events.<sup>17</sup> The detection of each individual current blockade in a nanopore current versus time recording is based on a single current-threshold ( $Th$ ) method. A blockade event is detected when the current magnitude becomes smaller than  $Th$ , until it returns to a value greater than  $Th$ . The beginning of the blockade is defined as the first point of current increase after having monotonically decreased below  $Th$ , and its end as the last point of current decrease before monotonically increasing above  $Th$ . This defines the range of points used to compute the characteristic quantities of the blockade, such as blockade duration  $t_b$ , mean value  $I_b$ , and standard deviation  $\sigma_b$  of the residual current. Here,  $Th = I_0 - 5\sigma_0$ , where  $I_0$  and  $\sigma_0$  are respectively the mean value and standard deviation of a Gaussian fit of the open-pore current distribution. Before detection of blockades, the nanopore current versus time trace is smoothed using a median filter, with a 13-point window.

Histograms of relative mean residual current  $I_b/I_0$  are constructed with a bin width of 0.005.  $I_b/I_0$  values constitute the main criterion to discriminate populations of blockades induced by enzymatically produced polypeptide fragments from the target proteins.  $I_b/I_0$  population  $j$  is defined as the subset of blockades whose  $I_b/I_0$  values fall in the range  $\langle I_b/I_0 \rangle_j \pm 1.96\sigma_j$ , where  $\langle I_b/I_0 \rangle_j$  and  $\sigma_j$  are the mean value and standard deviation of a Gaussian fit of the distribution of  $I_b/I_0$  values in the corresponding histogram peak, respectively. This range includes 95% of the Gaussian distribution.

The mean blockade duration  $\langle t_b \rangle_j$  is determined by fitting the distribution of  $\ln[\langle t_b \rangle_j]$  values with a single-exponential probability density model, where the maximum of the distribution occurs at  $\ln[\langle t_b \rangle_j]$ . The mean standard deviation of the residual current  $\langle \sigma_b \rangle_j$  is the mean value of a Gaussian fit of the distribution of  $\langle \sigma_b \rangle_j$  values. In the case where the distribution of  $\langle \sigma_b \rangle_j$  presents different subpopulations, each subpopulation is Gaussian-fitted and associated with its own mean value.

## ■ ASSOCIATED CONTENT

### SI Supporting Information

The Supporting Information is available free of charge at <https://pubs.acs.org/doi/10.1021/jacs.1c11758>.

$\alpha$ -Hemolysin preliminary experiments; experiment reproducibility; theoretical fragments; nanopore protein database; physical mechanisms of peptide capture (PDF)

## ■ AUTHOR INFORMATION

### Corresponding Authors

**John J. Kasianowicz** – Department of Physics, University of South Florida, Tampa, Florida 33620, United States; Freiburg Institute for Advanced Studies, Universität Freiburg, 79104 Freiburg, Germany; Email: [johnkasianowicz@mac.com](mailto:johnkasianowicz@mac.com)

**Fabien Piguet** – CY Cergy Paris Université, CNRS, LAMBE, Cergy 95000, France; Email: [fabien.piguet@u-cergy.fr](mailto:fabien.piguet@u-cergy.fr)

**Abdelghani Oukhaled** – CY Cergy Paris Université, CNRS, LAMBE, Cergy 95000, France; [orcid.org/0000-0002-9675-6747](https://orcid.org/0000-0002-9675-6747); Email: [abdelghani.oukhaled@cyu.fr](mailto:abdelghani.oukhaled@cyu.fr)

### Authors

**Mazdak Afshar Bakshloo** – CY Cergy Paris Université, CNRS, LAMBE, Cergy 95000, France

**Manuela Pastoriza-Gallego** – CY Cergy Paris Université, CNRS, LAMBE, Cergy 95000, France

**Jérôme Mathé** – Université Paris-Saclay, Univ Evry, CNRS, LAMBE, Evry-Courcouronnes 91000, France

**Régis Daniel** – Université Paris-Saclay, Univ Evry, CNRS, LAMBE, Evry-Courcouronnes 91000, France; [orcid.org/0000-0003-0725-5439](https://orcid.org/0000-0003-0725-5439)

Complete contact information is available at:

<https://pubs.acs.org/10.1021/jacs.1c11758>

## Notes

The authors declare no competing financial interest.

## ■ ACKNOWLEDGMENTS

This work was supported by the Agence Nationale de la Recherche ANR (ANR-17-CE09-0032-01 to A.O., M.P.-G., and F.P.), NIST Office of Law Enforcement Standards, and a Marie Skłodowska-Curie/Freiburg Institute for Advanced Studies Senior Fellowship (both to J.J.K.). We thank F. Gisou van der Goot (Ecole Polytechnique Federale de Lausanne, Switzerland) for providing the pET22b-proAL plasmid containing the proaerolysin sequence and Dr. Joseph Reiner (NIST) for performing the experiments with truncated lethal factor and the  $\alpha$ -hemolysin nanopore at our request.

## ■ REFERENCES

- (1) Marx, V. A Dream of Single-Cell Proteomics. *Nat. Methods* **2019**, *16* (9), 809–812.
- (2) O'Farrell, P. High Resolution Two-Dimensional Electrophoresis of Proteins. *J. Biol. Chem.* **1975**, *250* (10), 4007–4021.
- (3) Edman, P. Method for Determination of the Amino Acid Sequence in Peptides. *Acta Chem. Scand.* **1950**, *4* (7), 283–293.
- (4) Crowther, J. R. *ELISA: Theory and Practice*; Springer Science & Business Media, 1995; Vol. 42.
- (5) Tanaka, K.; Waki, H.; Ido, Y.; Akita, S.; Yoshida, Y.; Yoshida, T.; Matsuo, T. Protein and Polymer Analyses up Tom/z 100 000 by Laser Ionization Time-of-Flight Mass Spectrometry. *Rapid Commun. Mass Spectrom.* **1988**, *2* (8), 151–153.
- (6) Kopylov, A. T.; Zgoda, V. G.; Lisitsa, A. V.; Archakov, A. I. Combined Use of Irreversible Binding and MRM Technology for Low- and Ultralow Copy-Number Protein Detection and Quantitation. *Proteomics* **2013**, *13* (5), 727–742.
- (7) Archakov, A. I.; Ivanov, Y. D.; Lisitsa, A. V.; Zgoda, V. G. AFM Fishing Nanotechnology Is the Way to Reverse the Avogadro Number in Proteomics. *Proteomics* **2007**, *7* (1), 4–9.
- (8) Swaminathan, J.; Boulgakov, A. A.; Hernandez, E. T.; Bardo, A. M.; Bachman, J. L.; Marotta, J.; Johnson, A. M.; Anslyn, E. V.; Marcotte, E. M. Highly Parallel Single-Molecule Identification of Proteins in Zeptomole-Scale Mixtures. *Nat. Biotechnol.* **2018**, *36* (11), 1076.
- (9) van Ginkel, J.; Filius, M.; Szczepaniak, M.; Tulinski, P.; Meyer, A. S.; Joo, C. Single-Molecule Peptide Fingerprinting. *Proc. Natl. Acad. Sci. U. S. A.* **2018**, *115*, 3338–3343.
- (10) Bush, J.; Maulbetsch, W.; Lepoitevin, M.; Wiener, B.; Skanata, M. M.; Moon, W.; Pruitt, C.; Stein, D. The Nanopore Mass Spectrometer. *Rev. Sci. Instrum.* **2017**, *88*, 113307.
- (11) Zhao, Y.; Ashcroft, B.; Zhang, P.; Liu, H.; Sen, S.; Song, W.; Im, J.; Gyrfas, B.; Manna, S.; Biswas, S.; Borges, C.; Lindsay, S. Single-Molecule Spectroscopy of Amino Acids and Peptides by Recognition Tunnelling. *Nat. Nanotechnol.* **2014**, *9* (6), 466–473.
- (12) Ohshiro, T.; Tsutsui, M.; Yokota, K.; Furuhashi, M.; Taniguchi, M.; Kawai, T. Detection of Post-Translational Modifications in Single Peptides Using Electron Tunnelling Currents. *Nat. Nanotechnol.* **2014**, *9* (10), 835–840.
- (13) Alfaro, J. A.; Bohländer, P.; Dai, M.; Filius, M.; Howard, C. J.; van Kooten, X. F.; Ohayon, S.; Pomorski, A.; Schmid, S.; Aksimentiev,

- A.; Anslyn, E. V.; Bedran, G.; Cao, C.; Chinappi, M.; Coyaud, E.; Dekker, C.; Dittmar, G.; Drachman, N.; Eelkema, R.; Goodlett, D.; Hentz, S.; Kalathiya, U.; Kelleher, N. L.; Kelly, R. T.; Kelman, Z.; Kim, S. H.; Kuster, B.; Rodriguez-Larrea, D.; Lindsay, S.; Maglia, G.; Marcotte, E. M.; Marino, J. P.; Masselon, C.; Mayer, M.; Samaras, P.; Sarthak, K.; Sepiashvili, L.; Stein, D.; Wanunu, M.; Wilhelm, M.; Yin, P.; Meller, A.; Joo, C. The Emerging Landscape of Single-Molecule Protein Sequencing Technologies. *Nat. Methods* **2021**, *18* (6), 604–617.
- (14) Restrepo-Perez, L.; Joo, C.; Dekker, C. Paving the Way to Single-Molecule Protein Sequencing. *Nat. Nanotechnol.* **2018**, *13*, 786–796.
- (15) Bezrukov, S. M.; Kasianowicz, J. J. Current Noise Reveals Protonation Kinetics and Number of Ionizable Sites in an Open Protein Ion Channel. *Phys. Rev. Lett.* **1993**, *70* (15), 2352–2355.
- (16) Kasianowicz, J. J.; Burden, D. L.; Han, L. C.; Cheley, S.; Bayley, H. Genetically Engineered Metal Ion Binding Sites on the Outside of a Channel's Transmembrane L-Barrel. *Biophys. J.* **1999**, *76*, 9.
- (17) Kasianowicz, J. J.; Brandin, E.; Branton, D.; Deamer, D. W. Characterization of Individual Polynucleotide Molecules Using a Membrane Channel. *Proc. Natl. Acad. Sci. U. S. A.* **1996**, *93* (24), 13770–13773.
- (18) Kasianowicz, J. J.; Henrickson, S. E.; Weetall, H. H.; Robertson, B. Simultaneous Multianalyte Detection with a Nanometer-Scale Pore. *Anal. Chem.* **2001**, *73* (10), 2268–2272.
- (19) Robertson, J. W. F.; Rodrigues, C. G.; Stanford, V. M.; Rubinson, K. A.; Krasilnikov, O. V.; Kasianowicz, J. J. Single-Molecule Mass Spectrometry in Solution Using a Solitary Nanopore. *Proc. Natl. Acad. Sci. U. S. A.* **2007**, *104* (20), 8207–8211.
- (20) Baaken, G.; Ankri, N.; Schuler, A.-K.; Rühle, J.; Behrends, J. C. Nanopore-Based Single-Molecule Mass Spectrometry on a Lipid Membrane Microarray. *ACS Nano* **2011**, *5* (10), 8080–8088.
- (21) Baaken, G.; Halimeh, I.; Bacri, L.; Pelta, J.; Oukhaled, A.; Behrends, J. C. High-Resolution Size-Discrimination of Single Nonionic Synthetic Polymers with a Highly Charged Biological Nanopore. *ACS Nano* **2015**, *9* (6), 6443–6449.
- (22) Kullman, L.; Winterhalter, M.; Bezrukov, S. M. Transport of Maltodextrins through Maltoporin: A Single-Channel Study. *Biophys. J.* **2002**, *82* (2), 803–812.
- (23) Bacri, L.; Oukhaled, A.; Hémon, E.; Bassafoula, F. B.; Auvray, L.; Daniel, R. Discrimination of Neutral Oligosaccharides through a Nanopore. *Biochem. Biophys. Res. Commun.* **2011**, *412* (4), 561–564.
- (24) Oukhaled, G.; Mathé, J.; Bianche, A.-L.; Bacri, L.; Betton, J.-M.; Lairez, D.; Pelta, J.; Auvray, L. Unfolding of Proteins and Long Transient Conformations Detected by Single Nanopore Recording. *Phys. Rev. Lett.* **2007**, *98* (15), 158101.
- (25) Pastoriza-Gallego, M.; Rabah, L.; Gibrat, G.; Thiebot, B.; van der Goot, F. G.; Auvray, L.; Betton, J.-M.; Pelta, J. Dynamics of Unfolded Protein Transport through an Aerolysin Pore. *J. Am. Chem. Soc.* **2011**, *133* (9), 2923–2931.
- (26) Oukhaled, A.; Bacri, L.; Pastoriza-Gallego, M.; Betton, J.-M.; Pelta, J. Sensing Proteins through Nanopores: Fundamental to Applications. *ACS Chem. Biol.* **2012**, *7* (12), 1935–1949.
- (27) Ouldali, H.; Sarthak, K.; Ensslen, T.; Piguet, F.; Manivet, P.; Pelta, J.; Behrends, J. C.; Aksimentiev, A.; Oukhaled, A. Electrical Recognition of the Twenty Proteinogenic Amino Acids Using an Aerolysin Nanopore. *Nat. Biotechnol.* **2020**, *38* (2), 176–181.
- (28) Ettedgui, J.; Kasianowicz, J. J.; Balijepalli, A. Single Molecule Discrimination of Heteropolytungstates and Their Isomers in Solution with a Nanometer-Scale Pore. *J. Am. Chem. Soc.* **2016**, *138* (23), 7228–7231.
- (29) Schibel, A. E. P.; An, N.; Jin, Q.; Fleming, A. M.; Burrows, C. J.; White, H. S. Nanopore Detection of 8-Oxo-7,8-Dihydro-2'-Deoxyguanosine in Immobilized Single-Stranded DNA via Adduct Formation to the DNA Damage Site. *J. Am. Chem. Soc.* **2010**, *132* (51), 17992–17995.
- (30) Howorka, S.; Siwy, Z. Nanopore Analytics: Sensing of Single Molecules. *Chem. Soc. Rev.* **2009**, *38* (8), 2360.
- (31) Coulter, W. H. Means for Counting Particles Suspended in a Fluid. US2656508, 1953.
- (32) Reiner, J. E.; Balijepalli, A.; Robertson, J. W. F.; Campbell, J.; Suehle, J.; Kasianowicz, J. J. Disease Detection and Management via Single Nanopore-Based Sensors. *Chem. Rev.* **2012**, *112* (12), 6431–6451.
- (33) Bezrukov, S. M.; Vodyanoy, I.; Brutyan, R. A.; Kasianowicz, J. J. Dynamics and Free Energy of Polymers Partitioning into a Nanoscale Pore. *Macromolecules* **1996**, *29* (26), 8517–8522.
- (34) Kasianowicz, J. J.; Robertson, J. W. F.; Chan, E. R.; Reiner, J. E.; Stanford, V. M. Nanoscopic Porous Sensors. *Annual Rev. Anal. Chem.* **2008**, *1* (1), 737–766.
- (35) Yusko, E. C.; Prangio, P.; Sept, D.; Rollings, R. C.; Li, J.; Mayer, M. Single-Particle Characterization of A $\beta$  Oligomers in Solution. *ACS Nano* **2012**, *6* (7), 5909–5919.
- (36) Derrington, I. M.; Butler, T. Z.; Collins, M. D.; Manrao, E.; Pavlenok, M.; Niederweis, M.; Gundlach, J. H. Nanopore DNA Sequencing with MspA. *Proc. Natl. Acad. Sci. U. S. A.* **2010**, *107* (37), 16060.
- (37) Manrao, E. A.; Derrington, I. M.; Laszlo, A. H.; Langford, K. W.; Hopper, M. K.; Gillgren, N.; Pavlenok, M.; Niederweis, M.; Gundlach, J. H. Reading DNA at Single-Nucleotide Resolution with a Mutant MspA Nanopore and Phi29 DNA Polymerase. *Nat. Biotechnol.* **2012**, *30* (4), 349–353.
- (38) Kumar, S.; Tao, C.; Chien, M.; Hellner, B.; Balijepalli, A.; Robertson, J. W. F.; Li, Z.; Russo, J. J.; Reiner, J. E.; Kasianowicz, J. J.; Ju, J. PEG-Labeled Nucleotides and Nanopore Detection for Single Molecule DNasequencing by Synthesis. *Sci. Rep.* **2012**, *2* (1), 684.
- (39) Fuller, C. W.; Kumar, S.; Porel, M.; Chien, M.; Bibillo, A.; Stranges, P. B.; Dorwart, M.; Tao, C.; Li, Z.; Guo, W.; Shi, S.; Korenblum, D.; Trans, A.; Aguirre, A.; Liu, E.; Harada, E. T.; Pollard, J.; Bhat, A.; Cech, C.; Yang, A.; Arnold, C.; Palla, M.; Hovis, J.; Chen, R.; Morozova, I.; Kalachikov, S.; Russo, J. J.; Kasianowicz, J. J.; Davis, R.; Roeber, S.; Church, G. M.; Ju, J. Real-Time Single-Molecule Electronic DNA Sequencing by Synthesis Using Polymer-Tagged Nucleotides on a Nanopore Array. *Proc. Natl. Acad. Sci. U. S. A.* **2016**, *113* (19), 5233–5238.
- (40) Brinkerhoff, H.; Kang, A. S. W.; Liu, J.; Aksimentiev, A.; Dekker, C. Multiple Re-reads of Single Proteins at Single-Amino-Acid Resolution Using Nanopores. *Science* **2021**, *374* (6574), 1509–1513.
- (41) Yan, S.; Zhang, J.; Wang, Y.; Guo, W.; Zhang, S.; Liu, Y.; Cao, J.; Wang, Y.; Wang, L.; Ma, F.; Zhang, P.; Chen, H.-Y.; Huang, S. Single Molecule Ratcheting Motion of Peptides in a Mycobacterium Smegmatis Porin A (MspA) Nanopore. *Nano Lett.* **2021**, *21*, 6703.
- (42) Nivala, J.; Marks, D. B.; Akeson, M. Unfoldase-Mediated Protein Translocation through an  $\alpha$ -Hemolysin Nanopore. *Nat. Biotechnol.* **2013**, *31* (3), 247–250.
- (43) Kennedy, E.; Dong, Z.; Tennant, C.; Timp, G. Reading the Primary Structure of a Protein with 0.07 Nm<sup>3</sup> Resolution Using a Subnanometre-Diameter Pore. *Nat. Nanotechnol.* **2016**, *11* (11), 968–976.
- (44) Rodriguez-Larrea, D.; Bayley, H. Multistep Protein Unfolding during Nanopore Translocation. *Nat. Nanotechnol.* **2013**, *8* (4), 288–295.
- (45) Boersma, A. J.; Bayley, H. Continuous Stochastic Detection of Amino Acid Enantiomers with a Protein Nanopore. *Angew. Chem.* **2012**, *124* (38), 9744–9747.
- (46) Huang, G.; Voet, A.; Maglia, G. FraC Nanopores with Adjustable Diameter Identify the Mass of Opposite-Charge Peptides with 44 Da Resolution. *Nat. Commun.* **2019**, *10* (1), 835.
- (47) Piguet, F.; Ouldali, H.; Pastoriza-Gallego, M.; Manivet, P.; Pelta, J.; Oukhaled, A. Identification of Single Amino Acid Differences in Uniformly Charged Homopolymeric Peptides with Aerolysin Nanopore. *Nat. Commun.* **2018**, *9*, 966.
- (48) Chavis, A. E.; Brady, K. T.; Hatmaker, G. A.; Angevine, C. E.; Kothalawala, N.; Dass, A.; Robertson, J. W. F.; Reiner, J. E. Single Molecule Nanopore Spectrometry for Peptide Detection. *ACS Sensors* **2017**, *2*, 1319–1328.

- (49) Huang, G.; Willems, K.; Soskine, M.; Wloka, C.; Maglia, G. Electro-Osmotic Capture and Ionic Discrimination of Peptide and Protein Biomarkers with FraC Nanopores. *Nat. Commun.* **2017**, *8*, 935.
- (50) Zhao, Q.; Jayawardhana, D. A.; Wang, D.; Guan, X. Study of Peptide Transport through Engineered Protein Channels. *J. Phys. Chem. B* **2009**, *113* (11), 3572–3578.
- (51) Yuan, B.; Li, S.; Ying, Y.-L.; Long, Y.-T. The Analysis of Single Cysteine Molecules with an Aerolysin Nanopore. *Analyst* **2020**, *145* (4), 1179–1183.
- (52) Asandei, A.; Rossini, A. E.; Chinappi, M.; Park, Y.; Luchian, T. Protein Nanopore-Based Discrimination between Selected Neutral Amino Acids from Polypeptides. *Langmuir* **2017**, *33*, 14451–14459.
- (53) Restrepo-Pérez, L.; Huang, G.; Bohländer, P. R.; Worp, N.; Elkema, R.; Maglia, G.; Joo, C.; Dekker, C. Resolving Chemical Modifications to a Single Amino Acid within a Peptide Using a Biological Nanopore. *ACS Nano* **2019**, *13* (12), 13668–13676.
- (54) Nir, I.; Huttner, D.; Meller, A. Direct Sensing and Discrimination among Ubiquitin and Ubiquitin Chains Using Solid-State Nanopores. *Biophys. J.* **2015**, *108* (9), 2340–2349.
- (55) Hu, R.; Rodrigues, J. V.; Waduge, P.; Yamazaki, H.; Cressiot, B.; Chishti, Y.; Makowski, L.; Yu, D.; Shakhnovich, E.; Zhao, Q.; Wanunu, M. Differential Enzyme Flexibility Probed Using Solid-State Nanopores. *ACS Nano* **2018**, *12* (5), 4494–4502.
- (56) Rosen, C. B.; Rodriguez-Larrea, D.; Bayley, H. Single-Molecule Site-Specific Detection of Protein Phosphorylation with a Nanopore. *Nat. Biotechnol.* **2014**, *32* (2), 179–181.
- (57) Restrepo-Pérez, L.; Wong, C. H.; Maglia, G.; Dekker, C.; Joo, C. Label-Free Detection of Post-Translational Modifications with a Nanopore. *Nano Lett.* **2019**, *19* (11), 7957–7964.
- (58) Li, S.; Wu, X.; Li, M.; Liu, S.; Ying, Y.; Long, Y. T232K/K238Q Aerolysin Nanopore for Mapping Adjacent Phosphorylation Sites of a Single Tau Peptide. *Small Methods* **2020**, *4* (11), 2000014.
- (59) Ohayon, S.; Girsault, A.; Nasser, M.; Shen-Orr, S.; Meller, A. Simulation of Single-Protein Nanopore Sensing Shows Feasibility for Whole-Proteome Identification. *PLoS Comput. Biol.* **2019**, *15* (5), e1007067.
- (60) de Lannoy, C.; Lucas, F. L. R.; Maglia, G.; de Ridder, D. *In silico* assessment of a novel single-molecule protein fingerprinting method employing fragmentation and nanopore detection. *IScience* **2021**, *24* (10), 103202.
- (61) Swaminathan, J.; A, B. A.; Marcotte, E. M. A Theoretical Justification for Single Molecule Peptide Sequencing. *PLoS Computational Biology* **2015**, *11* (2), e1004080.
- (62) Yao, Y.; Docter, M.; van Ginkel, J.; de Ridder, D.; Joo, C. Single-Molecule Protein Sequencing through Fingerprinting: Computational Assessment. *Phys. Biol.* **2015**, *12* (5), 055003.
- (63) Yusko, E. C.; Bruhn, B. R.; Eggenberger, O. M.; Houghtaling, J.; Rollings, R. C.; Walsh, N. C.; Nandivada, S.; Pindrus, M.; Hall, A. R.; Sept, D.; Li, J.; Kalonia, D. S.; Mayer, M. Real-Time Shape Approximation and Fingerprinting of Single Proteins Using a Nanopore. *Nat. Nanotechnol.* **2017**, *12*, 360–367.
- (64) Bakshloo, M. A.; Talarimoghari, M.; Ouldali, H.; Behrends, J. C.; Oukhaled, A. Protein Fingerprinting Using the Aerolysin Nanopore. *Biophys. J.* **2020**, *118*, 475a.
- (65) Lucas, F. L. R.; Versloot, R. C. A.; Yakovlieva, L.; Walvoort, M. T. C.; Maglia, G. Protein Identification by Nanopore Peptide Profiling. *Nat. Commun.* **2021**, *12* (1), 5795.
- (66) Pannifer, A. D.; Wong, T. Y.; Schwarzenbacher, R.; Renatus, M.; Petosa, C.; Bienkowska, J.; Lacy, D. B.; Collier, R. J.; Park, S.; Leppa, S. H.; Hanna, P.; Liddington, R. C. Crystal Structure of the Anthrax Lethal Factor. *Nature* **2001**, *414* (6860), 229–233.
- (67) Ponomarenko, E. A.; Poverennaya, E. V.; Ilgisonis, E. V.; Pyatnitskiy, M. A.; Kopylov, A. T.; Zgoda, V. G.; Lisitsa, A. V.; Archakov, A. I. The Size of the Human Proteome: The Width and Depth. *International Journal of Analytical Chemistry* **2016**, *2016*, 7436849.
- (68) Henrickson, S. E.; Misakian, M.; Robertson, B.; Kasianowicz, J. J. Driven DNA Transport into an Asymmetric Nanometer-Scale Pore. *Phys. Rev. Lett.* **2000**, *85* (14), 3057–3060.
- (69) Ambjörnsson, T.; Apell, S. P.; Konkoli, Z.; Di Marzio, E. A.; Kasianowicz, J. J. Charged Polymer Membrane Translocation. *J. Chem. Phys.* **2002**, *117* (8), 4063–4073.
- (70) Lubensky, D. K.; Nelson, D. R. Driven Polymer Translocation Through a Narrow Pore. *Biophys. J.* **1999**, *77* (4), 1824–1838.
- (71) Boukhet, M.; Piguet, F.; Ouldali, H.; Pastoriza-Gallego, M.; Pelta, J.; Oukhaled, A. Probing Driving Forces in Aerolysin and  $\alpha$ -Hemolysin Biological Nanopores: Electrophoresis versus Electro-osmosis. *Nanoscale* **2016**, *8* (43), 18352–18359.
- (72) Degiacomi, M. T.; Iacovache, I.; Pernot, L.; Chami, M.; Kudryashev, M.; Stahlberg, H.; van der Goot, F. G.; Dal Peraro, M. Molecular Assembly of the Aerolysin Pore Reveals a Swirling Membrane-Insertion Mechanism. *Nat. Chem. Biol.* **2013**, *9* (10), 623–629.
- (73) Parker, M. W.; Buckley, J. T.; Postma, J. P. M.; Tucker, A. D.; Leonard, K.; Pattus, F.; Tsernoglou, D. Structure of the *It* Aeromonas Toxin Proaerolysin in Its Water-Soluble and Membrane-Channel States. *Nature* **1994**, *367*, 292–295.
- (74) Iacovache, I.; Degiacomi, M. T.; Pernot, L.; Ho, S.; Schiltz, M.; Dal Peraro, M.; van der Goot, F. G. Dual Chaperone Role of the C-Terminal Propeptide in Folding and Oligomerization of the Pore-Forming Toxin Aerolysin. *PLoS Pathogens* **2011**, *7* (7), e1002135.
- (75) Castañeda-Agulló, M.; del Castillo, L. M.; Whitaker, J. R.; Tappel, A. L. Effect of Ionic Strength on the Kinetics of Trypsin and Alpha Chymotrypsin. *J. Gen. Physiol.* **1961**, *44* (6), 1103–1120.

## Recommended by ACS

### Proteome-Scale Screening to Identify High-Expression Signal Peptides with Minimal N-Terminus Biases via Yeast Display

Patrick V. Holec, Michael E. Birnbaum, *et al.*

JUNE 10, 2022  
ACS SYNTHETIC BIOLOGY

READ 

### Enhanced Signal to Noise Ratio Enables High Bandwidth Nanopore Recordings and Molecular Weight Profiling of Proteins

Y. M. Nuwan D. Y. Bandara and Kevin J. Freedman

SEPTEMBER 15, 2022  
ACS NANO

READ 

### Counting Protein Number in a Single Cell by a Picoliter Liquid Operating Technology

Hailong Yu, Xiangmin Zhang, *et al.*

AUGUST 18, 2022  
ANALYTICAL CHEMISTRY

READ 

### Highly Robust *de Novo* Full-Length Protein Sequencing

Zhi-Biao Mai, Gong Zhang, *et al.*

FEBRUARY 16, 2022  
ANALYTICAL CHEMISTRY

READ 

Get More Suggestions >